Theoretical and experimental study of the longitudinal uniaxial stress dependence of *I-V* characteristics in GaAs-$Al_xGa_{1-x}As$-GaAs heterojunction barriers

S. S. Lu, K. R. Lee,[a] K. H. Lee, and M. I. Nathan
Department of Electrical Engineering, University of Minnesota, 200 Union Street S. E., Minneapolis, Minnesota 55455

M. Heiblum and S. L. Wright
IBM Thomas J. Watson Research Center, Yorktown Heights, New York 10598

(Received 3 July 1989; accepted for publication 29 January 1990)

Tunneling and thermionic emission through n^+-GaAs–*i*-$Al_xGa_{1-x}As$–*n*-GaAs heterojunction barriers are studied as a function of temperature from 77 to 200 K and as a function of externally applied uniaxial stress up to 10 kbar. A procedure to extract parameters for theoretical calculations is also proposed. The parameters extracted from the *I-V* characteristics of these heterostructures grown on (100) GaAs substrates with different aluminum mole fractions from 0.3 to 0.8 and thicknesses from 300 to 400 Å agree well with those of previous reports. The dependence of the *I-V* characteristics on uniaxial stress in the ⟨100⟩ direction perpendicular to the heterojunction plane has also been measured. The experimental results show good agreement with theoretical calculations assuming there is a linear stress-dependent decrease of the energy-band edges of the longitudinal *X* valleys (X_l) in AlGaAs with respect to the Γ valley in GaAs. The slope of the decrease is found to be 14 ± 2 meV/kbar. This results in an *X*-valley shear deformation potential of 9.6 ± 1.8 eV, which is believed to be the most accurate measured value to date.

I. INTRODUCTION

In the course of developing a technology for semiconductor-insulator-semiconductor field-effect transistors (SISFETs),[1] a report on the study of GaAs-$Al_xGa_{1-x}As$-GaAs heterostructures was given by Solomon, Wright, and Lanza.[2] Extensive efforts have also been made by other researchers to understand the transport properties of electrons across semiconductor heterojunction barriers both experimentally[3-6] and theoretically.[7-11] Proper understanding of these barriers becomes very crucial to optimize ultrahigh-speed electronic devices using them.[12] In the *n*-doped-GaAs–undoped $Al_xGa_{1-x}As$–*n*-doped-GaAs double heterojunction, single-tunnel barrier, depending on the aluminum mole fration *x*, the Γ, *X*, and, perhaps, the *L* valleys in *k* space of the AlGaAs layer will be involved in the tunneling. Furthermore, the individual *X* and *L* valleys can contribute differently depending on their orientation with respect to the current direction. For tunneling in the ⟨100⟩ direction through *X* valleys, for example, there are two different orientations, i.e., two longitudinally oriented *X* valleys (X_l) with high mass $\sim m_0$ (m_0 is the free-electron mass) and four transversely oriented *X* valleys (X_t) with smaller mass $\sim 0.2m_0$ in the current direction. There is evidence that in some cases the latter dominates over the former,[2,4,5] and the role of X_l is not clear yet. This is because, while the tunneling mass through X_t is much smaller compared to that through X_l, tunneling through X_l can be favored by the momentum conservation perpendicular to the tunneling direction.

To understand these complex transport properties, many people have tried different methods. The *I-V* characteristics due to the thermionic emission (TE) as well as Fowler–Norheim tunneling (FN) currents with varying *x* are reported in Ref. 2, which shows clear evidence that both TE and FN are from Γ in GaAs to Γ in $Al_xGa_{1-x}As$ for low-*x* devices and are from Γ in GaAs to X_t in $Al_xGa_{1-x}As$ for high-*x* devices. Moreover, hydrostatic-pressure-dependent *I-V* characteristics of resonant tunneling diodes also support the above argument.[5,13] However, the role of X_t in $Al_xGa_{1-x}As$ in the electron transport may be more and more important as the thickness of the barrier decreases, as shown by a recent experiment.[6]

In this paper uniaxial-stress-dependent *I-V* characteristics of n^+-GaAs–*i*-$Al_xGa_{1-x}As$–*n*-GaAs double-heterojunction single-tunnel barriers are measured at 77 K and compared with theoretical calculations. Our stress is compressive and applied longitudinally along the ⟨100⟩ direction perpendicular to the heterojunction barrier by means of a push rod with a lever system.[14] This study relies on the fact that uniaxial stress along ⟨100⟩ can remove the degeneracy of *X* valleys.[15,16] Thus, when uniaxial stress is applied in the ⟨100⟩ direction, the minimum energy of X_t will increase compared to that of Γ, while that of X_l will decrease, enabling us to separate the current components flowing through each valley. The results of our measurement and calculation are that we are able to demonstrate the usefulness of uniaxial stress in elucidating the transport mechanisms in heterojunction barriers. We directly observed the suprising and new result that, for Fowler–Norheim tunneling, under appropriate conditions, the final state is not the lowest-energy valley, but the higher valley favored by smaller effective mass and momentum conservation. For the case of thermionic emission, in which thermally activated

[a] Permanent address: Department of Electrical Engineering, Korea Advanced Institute of Science and Technology, Cheongryang, Seoul, Korea.

 0021-8979/90/106360-08$03.00

electrons are emitted over a small barrier, the lowest energy tends to dominate. Moreover, from the stress-dependent barrier height, we can deduce the X-valley shear deformation potential, Ξ.[17]

In Sec. II, the method of the theoretical calculation of I-V characteristics will be described. Our experimental methods and results will be presented in Sec. III. This will be followed by discussion in Sec. IV and conclusions in Sec. V.

II. THEORETICAL CALCULATION OF I-V CHARACTERISTICS IN n^+-GaAs-i-$Al_xGa_{1-x}As$-n-GaAs SEMICONDUCTOR HETEROJUNCTION TUNNEL DIODES

The current density J emitted from either a metal or a semiconductor across an insulator with an energy barrier at the interface has long been well understood.[19] For the emission across the semiconductor heterojunction barrier under forward bias shown in Fig. 1, however, there can be many sets of nonequivalent valleys indexed by i in AlGaAs through which the currents J_i can flow. In other words,

$$J = \sum_i J_i$$

$$= e \sum_i N_i \int_{E_{ci}(0)}^{\infty} D_i(E_x) F(E_x)\, dE_x, \tag{1}$$

where e is the electronic charge, N_i is the number of equivalent valleys, $D_i(E_x)$ is the quantum-mechanical transmission probability, $F(E_x)dE_x$ is the net flux of electrons in the energy range between E_x and $E_x + dE_x$ incident on the surface per second per unit area, E_x is the energy of electrons in GaAs given by the sum of the potential energy and the component of the kinetic energy in the current direction, $E_{ci}(0)$ is the bottom of the conduction band in the low-gap material at the heterointerface, and the summation is over all sets of nonequivalent valleys. Using Fermi–Dirac statistics, the function $F(E_x)$ can be derived very easily to be

$$F(E_x) = \frac{4\pi m_{\Gamma} kT}{h^3} \ln\left(\frac{1 + \exp\left(\frac{E_{Fi} - E_x}{kT}\right)}{1 + \exp\left(\frac{E_{Fi} - E_x - V_A}{kT}\right)} \right). \tag{2}$$

Here m_{Γ} is the electron effective mass of the Γ valley in GaAs, kT is the thermal energy, h is Planck's constant, V_A is the applied voltage, and E_{Fi} is the Fermi energy. However, compared to the metal-insulator-metal structures, the quantum-mechanical calculation of $D_i(E_x)$ in semiconductor heterojunctions has been shown to be very complex, especially for the transmission through the valleys in AlGaAs which does not conserve the transverse crystal momentum.[7–9] In a relatively thick barrier with a triangular shape, however, the transmission probability $D_i(E_x)$ can be written as given below.[8,9,19] For $E_x < \phi_{B_i} - \Delta\phi_i$,

$$D_i(E_x) = B_i(E_x) \exp\left[-\frac{8\pi\sqrt{2m_i(\phi_{B_i} - E_x)^3}}{3heF} \times v\left(\frac{\Delta\phi_i}{\phi_{B_i} - E_x}\right) \right],$$

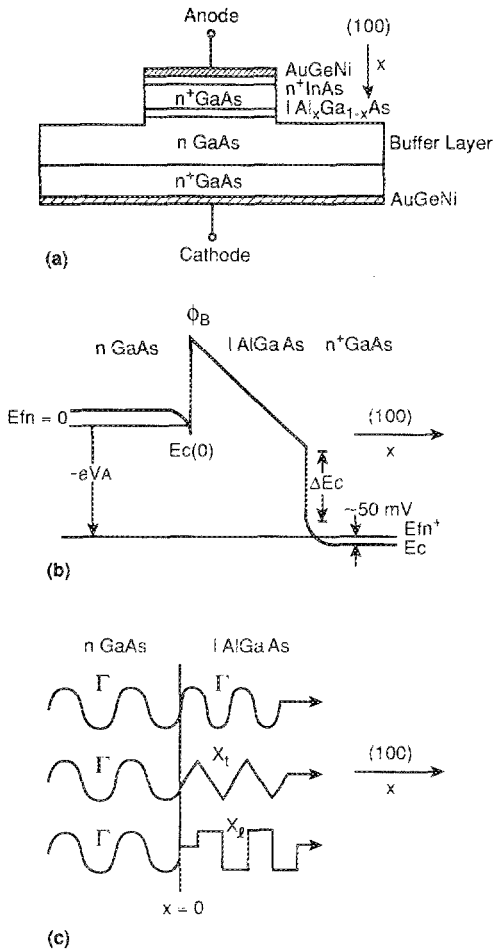

FIG. 1. (a) Cross section of the device structures studied in this work. The characteristics of the epitaxial growth are summarized in Table I. (b) Energy-band diagram at forward bias. (c) Diagrammatic representations of the electron transmission through Γ, X_t, and X_l valleys in AlGaAs layer (Ref. 6).

and for $E_x > \phi_{B_i} - \Delta\phi_i$,

$$D_i(E_x) = B_i(E_x), \tag{3}$$

$$\tag{4}$$

where $B_i(E_x)$ is the preexponential factor, m_i is the effective mass in the current direction, ϕ_{B_i} is the barrier height given by $\Delta E_{ci} - [E_{Fi} - E_{ci}(0)]$ where ΔE_{ci} is the conduction band discontinuity, F is the electric field intensity, $\Delta\phi_i$ is the barrier lowering due to the image force, and v is the correction factor due to $\Delta\phi_i$. Because $B_i(E_x)$ is almost impossible to find experimentally, we assume it independent of E_x as has been done before.[2,4] Then the resulting expression of Eq. (1) becomes

$$J = \sum_i (J_i^{\mathrm{TU}} + J_i^{\mathrm{TE}}), \tag{5}$$

where the tunneling current J_i^{TU} is given by

$$J_i^{\mathrm{TU}} = eB_i \int_{E_{ci}(0)}^{\phi_{B_i} - \Delta\phi} CF\, 1 exp\left(-\frac{8\pi\sqrt{2m_i(\phi_{B_i} - E_x)^3}}{3heF} v \right) \times F(E_x)\, dE_x, \tag{6}$$

and the thermionic emission current J_i^{TE} over the barrier is

given by

$$J_i^{\mathrm{TE}} = A_i N_i m_{di} T^2 \exp[-(\phi_{B_i} - \Delta\phi_i)/kT]. \quad (7)$$

Here m_{di} is the density-of-states effective mass in AlGaAs in units of m_0. In the limit of large ϕ_{B_i} at high field, Eq. (6) reduces to the following well-known Fowler-Nordheim current J_i^{FN}:[19]

$$J_i^{\mathrm{FN}} = \frac{B_i e^3 F^2}{8\pi h \phi_{B_i}} \exp\left(-\frac{8\pi\sqrt{2m_i}\phi_{B_i}^3}{3heF}\right). \quad (8)$$

In a semiconductor heterojunction barrier, the following problems prevent us from using simple equations like Eqs. (7) and (8) to analyze the measured data.

(i) The magnitude of ϕ_{B_i} is dependent on bias V_A or equivalently on F because of the band bending in GaAs.

(ii) Because of (i) F cannot be simply given by V_A/t as in the case of metal-insulator-metal structures, where t is the thickness of the barrier.

(iii) ϕ_{B_i} is relatively small, so that the validity of Eq. (8) is questionable.

(iv) There are many current components as can be seen in Eq. (5). It is not easy to separate them.

(v) The values of constants B_i, A_i, and m_i are in general not well known.

(vi) To find $E_{ci}(0)$ in Eq. (6) which depends on the bias, Poisson's equation should be solved. But it is not clear whether three-dimensional Fermi statistics or two-dimensional Fermi statistics should be used in the accumulation region where the electronic motion can be quantized. The values of $E_{ci}(0)$ calculated by the above two different approaches were shown to be very different.[20,21] But recent calculations[22-24] show that the difference between them is almost negligible. Thus in this work three-dimensional Fermi statistics are used to solve Poisson's equation assuming local equilibrium. As will be shown later, this gives good agreement between theory and experiment of our I-V data.

III. UNIAXIAL STRESS-DEPENDENT I-V CHARACTERISTICS: EXPERIMENTAL METHOD AND RESULTS

Compared to stress-dependent bulk piezoresistance measurements,[16,17,25] it is very difficult to apply uniform stress to our samples, because the active part of our device is very close to the surface. Traditional AuGeNi alloyed ohmic contacts cannot be used for our purpose because of the bad surface morphology after alloying, which leads to serious nonuniform stress. Therefore, we used a nonalloyed ohmic contact, which consists of molecular beam epitaxy growth of n^+-InAs over the n^+-GaAs top layer and AuGeNi metallization.

Our stress apparatus is very similar to that used before,[14] and stress was applied parallel to the current direction, that is, normal to the heterojunction by putting weight on a push rod with a lever system. Our anvil, made of tungsten carbide and polished optically flat using 1-μm diamond paste, was inserted into the push rod. Stress is applied to the top ohmic contact of one of the many devices fabricated on an approximately $\sim 5\times 5$-mm^2 sized substrate and isolated by ~ 2-μm mesa etching. Even with a nonalloyed ohmic contact, we found it difficult to obtain uniform stress. In some cases, the measured I-V characteristics looked like the sum of the current through a localized stressed area and that through a large unstressed area. We found, however, that in addition to the nonalloyed contact, using a ball of In-Ga mixture (75:25, 99.9999%), which is liquid at room temperature and is solid at 77 K, between the anode as shown in Fig. 1(a) and the anvil surfaces gave very repeatable and reversible measurement results. The hysteresis observed in the I-V characteristics is negligibly small. The detailed procedures are as follows: First, a small amount of In-Ga liquid metal was applied on the ~ 300-μm-diam anvil surface. Second, the anvil was inserted into the push rod, which was lowered carefully until In-Ga metal covered the entire 200-μm contact area. Third, samples were cooled slowly down to 77 K by raising the liquid-nitrogen Dewar slowly. Then I-V characteristics were measured at each stress level determined by the net weight divided by the contact area.

TABLE I. Characteristics of four n^+-GaAs–i-Al$_x$Ga$_{1-x}$As–n-GaAs heterostructure samples studied in our work.

Sample	n^+ top layer doping (cm^{-3})	Barrier: Aluminum composition x	Barrier: Thickness (Å)	Buffer doping (cm^{-3})
A	1×10^{18}	0.30	300	1×10^{16}
B	1×10^{18}	0.32	400	1×10^{18}
C	1×10^{18}	0.5	350	1×10^{16}
D	1×10^{18}	0.8	400	1×10^{16}

To extract parameters for our theoretical calculations the temperature dependence of the C-V and the I-V characteristics of many n^+-GaAs–i-Al$_x$Ga$_{1-x}$As–n-GaAs heterostructure samples grown by molecular beam epitaxy on (100) n^+-GaAs wafers were measured. The characteristics of the layers' physical properties are summarized in Table I. The buffer layer thickness is about 0.6 μm for all samples. All samples are circular mesas with 2 μm height and 200 μm diameter. Some samples were mounted on headers and wire bonded for temperature-dependent measurement. The doping density of the n-GaAs region is extracted from the deep depletion C-V characteristics. To characterize the measured I-V data from each sample, the following procedures are used.

(i) Find the apparent barrier height ϕ_{BR} and A_i from the current at reverse bias divided by T^2 vs $1/T$ plot from Eq. (7). At reverse bias, for n^+-i-n^- structures, most of the applied bias is dropped across the n^- depletion region. Therefore the electric field is small and tunneling is negligible. Moreover, $\Delta\phi_i$ is negligible and the conduction-band discontinuity ΔE_{ci} can be calculated by the sum of ϕ_{B_i} found from Eq. (7) and the equilibrium Fermi energy of n^+-GaAs relative to the conduction-band edge, which is about 50 meV. These values are listed under reverse I-V characteristics in Table II.

(ii) For the forward-biased regimes [see Figs. 1(a) and 1(b) caption], instead of a FN plot, where the measured

TABLE II. Summary of the apparent barrier heights ϕ_{BR} and ϕ_{BF}, the conduction-band discontinuities ΔE_{ci}, and prefactors for the dominant current transport mechanisms, deduced by the extraction methods described in Sec. II.

Sample ID	Reverse I-V characteristics			Forward I-V characteristics			Tunneling mass (m_0)
	ϕ_{BR} (eV)	ΔE_{ci} (eV)	A_i	ϕ_{BF} (eV)	ΔE_{ci} (eV)	B_i	
A	0.20	0.25	0.1	0.22	0.25	0.4	$m_\Gamma = 0.092$
B				0.25	0.28	0.4	$m_\Gamma = 0.094$
C	0.27	0.32	0.0015	0.37	0.40	0.4	$m_\Gamma = 0.109$
D	0.14	0.19	0.0015	0.17	0.20	0.00012	$m_t = 0.20$

current divided by F^2 vs $1/F$ is plotted (in Ref. 2, the field in AlGaAs is calculated at each bias point), we propose an equivalent FN (EFN) plot, where I/V_A^2 vs $1/V_A$ is plotted.[3] Thus V_A/t replaces F in Eq. (8). From the EFN of our calculated curves, we find that for a wide range of variation of t and ΔE_{ci} at $T = 77$ K, the apparent barrier height ϕ_{BF} found from the slope of the linear portion of the EFN is smaller by about 30 meV than ΔE_{ci}. In addition, a prefactor exaggerates B_i by about 1.5 times. The EFN plots of our samples are shown in Fig. 2 and the resulting values of ΔE_{ci} obtained by adding 30 meV to the calculated apparent barrier heights ϕ_{BF} and the B_i are listed under forward I-V characteristics in Table II.

As can be seen from Fig. 2 and Table II, for samples A and D, the ΔE_{ci}'s found from the above procedures agree well with each other, if we use $m_i = m_\Gamma$ for sample A and $m_t = 0.2m_0$ for sample D in Eq. (6).

However, the B_i for sample D is about 4000 times smaller than that for samples A and B. This agrees well with previous results[2,4] and has been attributed to tunneling through X_t in AlGaAs. Furthermore, A_i of sample D is also found to be about 670 times smaller than that of sample A. Note that there are four X_t, each with density-of-states mass of about $0.45m_0$ and two X_l, each with that of about $0.20m_0$, the sum of which can lead to about a 22 times smaller prefactor for TE through Γ than TE through X valleys in AlGaAs if one uses $m_\Gamma = 0.1m_0$. Sample C, however, does not show the same ΔE_{ci}'s found from the reverse and forward I-V characteristics. While ΔE_{ci} calculated from reverse-bias TE current is about 0.32 eV, as can be seen from Fig. 2, the forward I-V characteristic shows Γ-Γ tunneling with $\Delta E_{ci} \simeq 0.40$ eV and prefactor $\simeq 0.4$, which shows evidence for Γ-Γ tunneling. Although using $m_i = m_t = 0.20m_0$ to

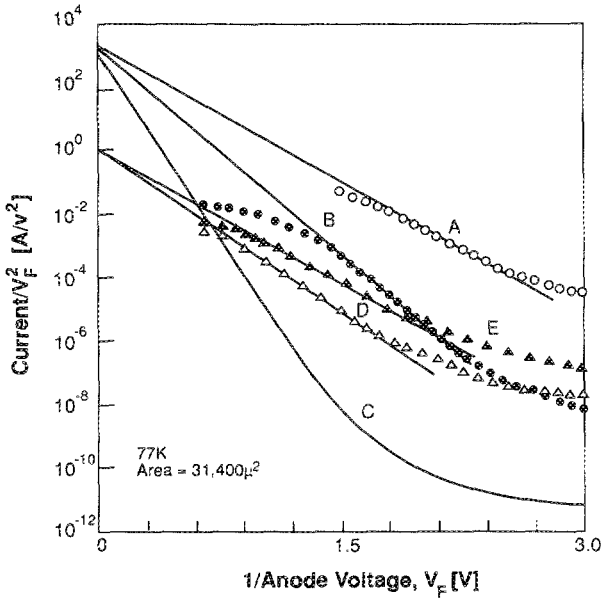

FIG. 2. Zero-stress equivalent Fowler–Nordheim plot (EFN) at 77 K of five devices fabricated in our lab. The open circles are measured points for sample A, solid circles for B, solid curved line for C, open triangles for D, and solid triangles for E, which has the same growth characteristics as D except $t = 300$ Å, respectively. From the slope and y intercept of the linear extrapolated lines, ϕ_{BF} and B_i in Table II are determined.

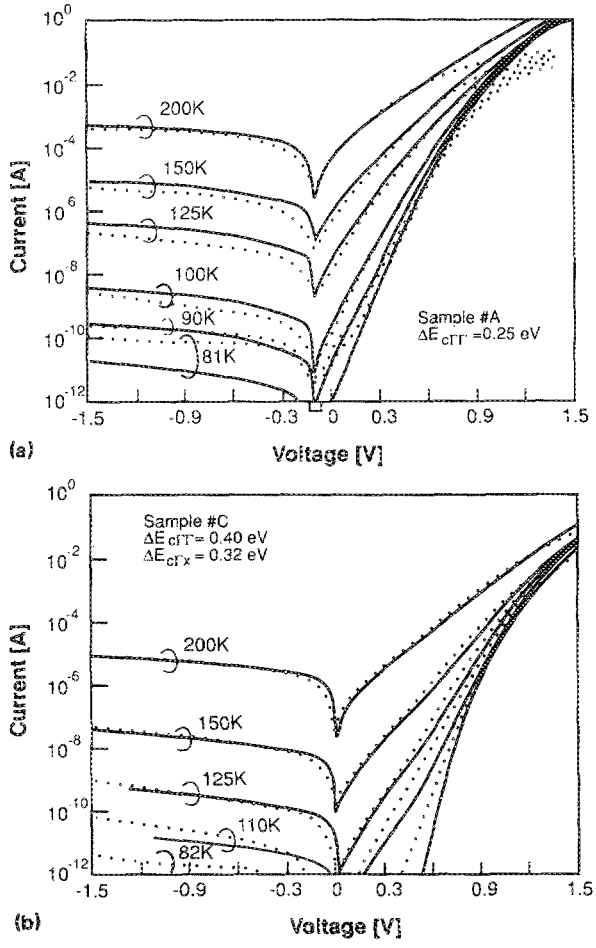

FIG. 3. Experimental (dots) and theoretical (solid lines) temperature dependent I-V characteristics of (a) sample A and (b) sample C.

calculate ϕ_{BF} leads to $\Delta E_{ci} \cong 0.32$ eV, from the prefactor of this device as large as those of samples A and B, we can conclude that the forward I-V characteristic for sample C is dominated by a Γ-Γ tunneling ($V \geqslant 0.8$), while the reverse I-V characteristic is dominated by TE in X valleys. This apparently different dominant current component between the reverse and forward I-V characteristics is quite in contrast with the previous result,[2] which found almost the same ΔE_{ci}'s for both current directions. Note that all values of ΔE_{ci} listed in Table II agree well with those expected from the aluminum concentration x.[26]

Figure 3 compares experimental and theoretical temperature-dependent I-V characteristics for samples A and C. The calculation is done by integrating Eq. (6) numerically using extracted parameters listed in Table II. As can be seen from Fig. 3, the agreement between experiment and theory is excellent for the entire range of temperature and applied voltage except that the TE at low temperature (i.e., 82 and 81 K) for both samples does not follow Eq. (7). This implies that there are other excess current components dominant at low temperature and independent of temperature. One possibility is tunneling through impurities in AlGaAs.[4,10]

Figure 4(a) shows experimental results for sample B, which has the following remarkably interesting features.[27] At low stress, the I-V characteristic does not change with stress at all. As we increase the stress, the current at low voltage increases very rapidly, while the current at high voltage remains the same. Because this sample shows symmet-

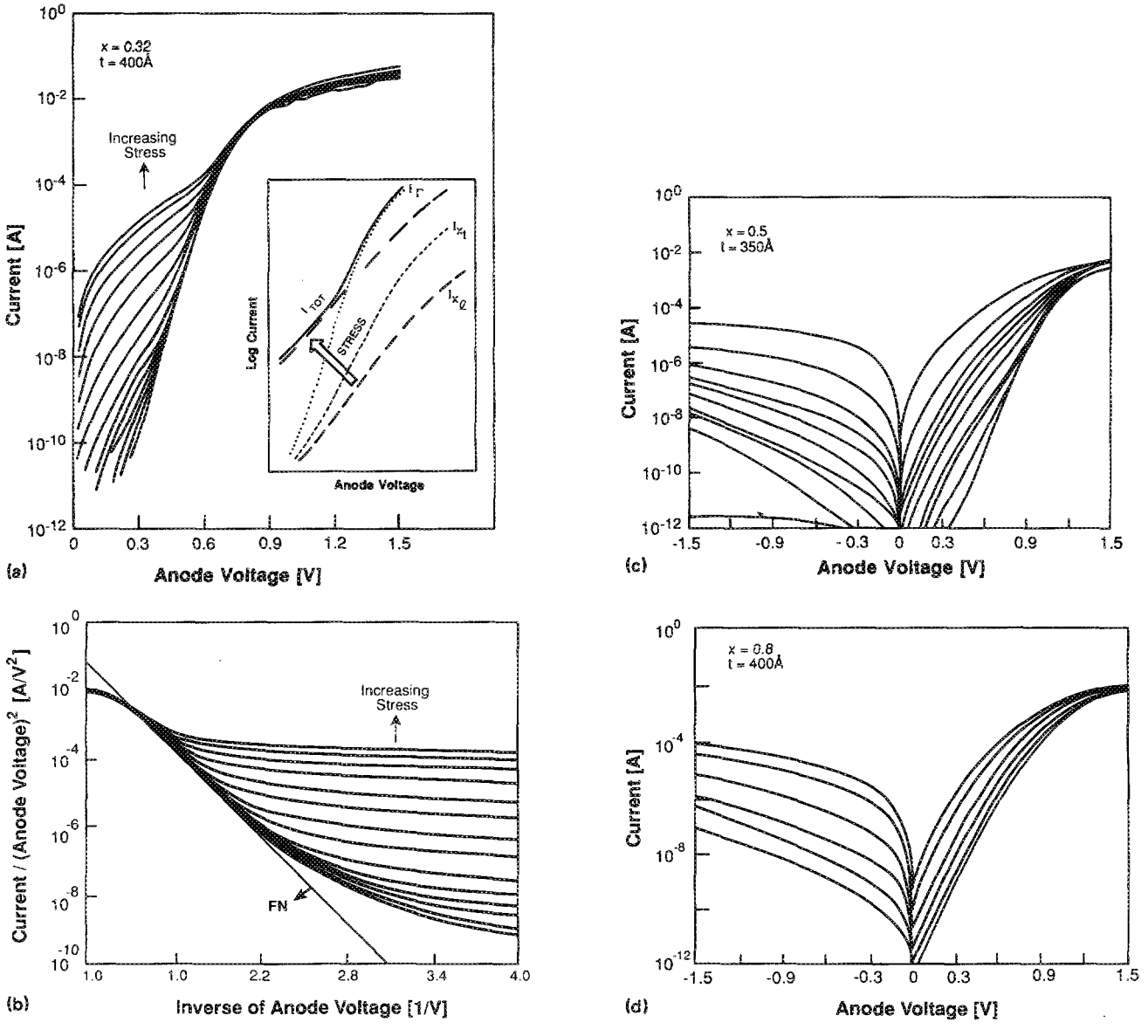

FIG. 4. Measured I-V characteristics at 77 K with net weight as a parameter (Ref. 27). The stressed area is circular with 200 μm diameter in all cases. (a) I-V characteristics of sample B. Bottom curve corresponds to zero to 2.6 kbar and top curve to 10.6 kbar with a 0.62-kbar step. Inset shows the total current I_Γ at zero stress (dotted line) is all associated with the Γ minimum. At high stress the total current, (I_{TOT}, solid line) is composed of three components, current through Γ valley in AlGaAs (I_Γ, dotted line), through X_t (I_{X_t}, dashed line) and through X_l (I_{X_l}, heavy dashed line). Under uniaxial stress along ⟨100⟩, only I_{X_l} increases appreciably. (b) Effective Fowler–Nordheim plot of (a). Parameter values are the same as in (a). (c) I-V characteristics of sample C (bottom, zero; top, 6.8 kbar; first seven steps, 0.62 kbar; last two steps, 1.24 kbar). (d) I-V characteristics of sample D (bottom, zero; top, 3.1 kbar; step, 0.62 kbar).

ric I-V characteristics, only forward I-V characteristics are shown here. The EFN plot of these data is shown in Fig. 4(b).

Figures 4(c) and 4(d) show I-V characteristics with stress as a parameter for samples C and D, respectively. Because these samples are doped asymmetrically, we observe TE at reverse bias and TE and FN at forward bias. The major difference of the stress dependence of samples C and D from that of B is that the TE currents start to increase rapidly as soon as stress is applied. The details of our analysis will be discussed in the next section.

IV. DISCUSSION

The stress-dependent I-V characteristics of sample B, which is shown in Fig. 4(a), can be attributed to the crossover of Γ and X_l in AlGaAs. According to the data reported in Ref. 26, the energy of Γ in AlGaAs for the $x = 0.32$ sample is lower than that of X by about 70 meV at zero stress. When uniaxial stress is applied in the $\langle 100 \rangle$ direction, the Γ minimum in AlGaAs will move almost at the same rate as that in GaAs.[28,29] In other words,

$$\delta(E_1^{\Gamma} - E_0^{\Gamma})/\delta S \approx 0, \tag{9}$$

where S is the stress and E_1^{Γ} and E_0^{Γ} are the Γ energy minima in AlGaAs and GaAs, respectively. On the other hand, the X-valley minima will split and X_l and X_t will move at different rates[16]:

$$\delta(E_1^{X_l} - E_0^{\Gamma})/\delta S = \tfrac{1}{3}\delta(E_1^{X} - E_0^{\Gamma})/\delta P - \tfrac{2}{3}\Xi_u^X(S_{11} - S_{12}), \tag{10}$$

$$\delta(E_1^{X_t} - E_0^{\Gamma})/\delta S = \tfrac{1}{3}\delta(E_1^{X} - E_0^{\Gamma})/\delta P + \tfrac{1}{3}\Xi_u^X(S_{11} - S_{12}). \tag{11}$$

Here P is the hydrostatic pressure, Ξ_u^X is the shear deformation potential of the X valleys in AlGaAs, S_{11} and S_{12} are components of the compliance tensor, E_1^X is the energy minima of X valleys under hydrostatic pressure, and $E_1^{X_l}$ and $E_1^{X_t}$ are the energy minima of X_l and X_t, respectively. If we use $\delta(E_1^X - E_0^{\Gamma})/\delta P = -12.0$ meV/kbar,[28,29] $S_{11} = 1.17\times10^{-6}$ bar^{-1}, $S_{12} = -0.37\times10^{-6}$ bar^{-1} of GaAs, and $\Xi_u^X = 8.6$ eV of silicon, which is not well known for GaAs,[18] from Eqs. (10) and (11) we can deduce that $E_1^{X_l} - E_0^{\Gamma}$ and $E_1^{X_t} - E_0^{\Gamma}$ move at rates of -13 meV/kbar and 0.4 meV/kbar, respectively. This is illustrated in Fig. 5.

Because E_1^X is higher than E_1^{Γ} by about 70 meV for sample B at zero stress, we can see that about 5 kbar is necessary to get the energy crossover of Γ and X_l. As will be shown later, however, rigorous calculation shows that about 10 kbar are necessary to get the current crossover. This explains why the I-V characteristics do not change at all at low stress in Fig. 4(a). Moreover, as stress increases further, $E_1^{X_l}$ becomes smaller than E_1^{Γ}. When this happens, TE through X_l is dominant over TFE through Γ. But at high bias Fowler–Nordheim tunneling (FN) through Γ is still dominant over TE through X_l. This is because the tunneling mass of X_l is much larger than that of Γ. This can be seen better in an EFN plot as shown in Fig. 4(b). We can see from the EFN plot that FN dominates at high voltage and TE dominates at low voltage at all values of stress. At zero stress all currents are through Γ in AlGaAs. But as stress increases, TE through X_l increases rapidly and becomes dominant, while FN through Γ stays the same. This is consistent with Eqs. (9) and (10), and is illustrated in the inset of Fig. 4(a), which shows the three current components through each valley and the increase of the current through X_l under uniaxial stress.[27] The currents through Γ and X_t remain almost constant. The change in current versus stress for sample B at a fixed voltage is shown in Fig. 6. As has been pointed out earlier,[19] for TE, the current at a fixed voltage is proportional to $\exp(-\phi_{B_l}/kT)$. $\delta\phi_{B_l}/\delta S$ of -13 meV/kbar is obtained from the slope in Fig. 6 (TE is dominant). This agrees

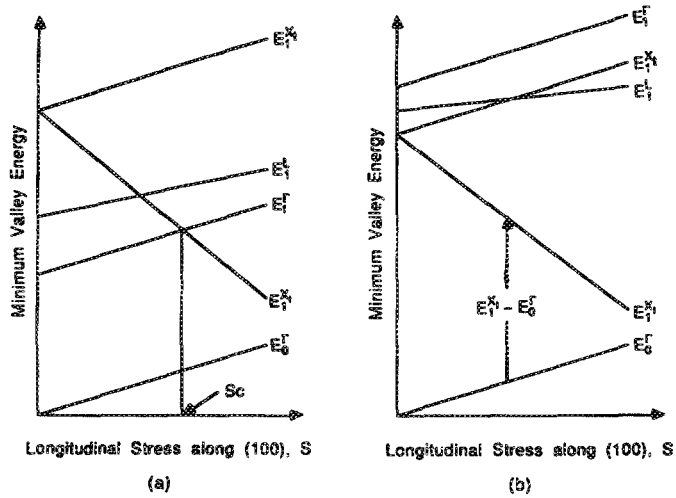

FIG. 5. Movement of the conduction-band edge energies under uniaxial stress of (a) low-x device where S_c is the critical stress point for E_1^{Γ} and $E_1^{X_l}$ crossover and (b) high-x device.

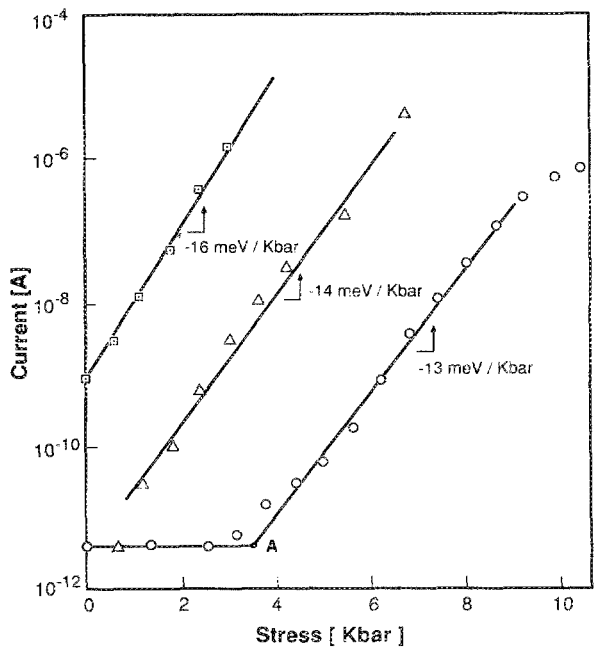

FIG. 6. Log of current vs stress at fixed voltages from the data in Fig. 4. Open circles are for sample B measured at 0.25 V, open triangles for sample C, and open squares for sample D measured at 0.3 V, respectively. Point marked as A is the critical stress point for the current crossover of sample B.

with $\delta(E_1^{X_l} - E_0^{\Gamma})/\delta S$ in Eq. (10). It is interesting to notice that this value of slope coincides with that obtained using the Si deformation potential. However, the critical stress obtained from Fig. 6 is about 4 kbar, which is much less than the 10 kbar calculated for sample B from x, Ξ, and prefactors of X_l and Γ. In other words, $\delta(E_1^{X_l} - E_0^{\Gamma})/\delta S$ obtained from the decreasing of barrier height is different from that to get crossover of the currents through Γ and X_l in AlGaAs.

The stress-dependent current characteristics at fixed voltages for samples C and D are also shown in Fig. 6. The largest difference of sample C and D data from that of sample B is that the TE starts to increase rapidly as soon as stress is applied. This coincides with the hydrostatic pressure results reported earlier[13] and indicates that X valleys are the lowest conduction band at zero stress. The rates of barrier lowering $\delta(E_1^{X_l} - E_0^{\Gamma})/\delta S$ calculated from the slopes in Fig. 6 are -14 and -16 meV/kbar for samples C and D, respectively. These values are very close to that found for sample B which, if we assume constant Ξ_u^X in AlGaAs independent of x, indicates the stresses are fairly uniform.

If we insert the measured average value of 14 ± 2 meV/kbar as $\delta(E_1^{X_l} - E_0^{\Gamma})/\delta S$ into Eq. (10), we find the X-valley shear deformation potential to be 9.6 ± 1.8 eV. This value is closer to the corresponding deformation potential constant for Si (8.6 eV) than that for GaP (6.9 eV), but much less than previously reported values as suspected in Ref. 17. As far as we know, our result of 9.6 ± 1.8 eV is the most accurately measured value of X-valley shear deformation potential to date,[27] which, however, may depend on the aluminum composition x.

The calculated I-V characteristics using the theory developed in Sec. II are shown in Fig. 7 for samples B, C, and D. The conduction-band discontinuity, $E_1^{X_l} - E_0^{\Gamma}$, is taken as a parameter. As can be seen from Figs. 4 and 7, we can replicate the experimental results well by a theoretical calculation. But for samples B and C, we have to assume about a 80 meV smaller absolute value of $E_1^{X_l} - E_0^{\Gamma}$. For sample B, the energy offset of 80 meV required to match curves in Figs. 4(a) and 7(a) appears as about a 6-kbar difference between theoretical and experimental values of crossover stress. At this moment, this difference is not understood. There appear to be at least three possible explanations. One is the tunneling through impurities in AlGaAs,[4] which may be mixed with X valleys. This explanation may be reasonable because as can be seen from Fig. 3, these two samples show anomalously large zero-bias conductance at low temperature. A second explanation is the errors in the measurement of the Al mole fraction and conduction-band edge discontinuity as discussed by Kuech *et al.*[30] and Theis.[31] A third possibility is that the stress is nonuniform at low stress but becomes uniform at high stress. The fact that the data look the same for two B samples suggests the last explanation is least likely. On the other hand, if we extrapolate the thermionic emission current through X_l of sample B to zero stress in Fig. 6 and use the fact that current crossover happens at about 4 kbar and $\delta(E_1^{X_l} - E_0^{\Gamma})/\delta S = -14$ meV/kbar, we deduce that $\Delta E_{\Gamma X}$ is 0.29 eV, which is somewhat lower than those obtained by other researchers. The agreement between theory

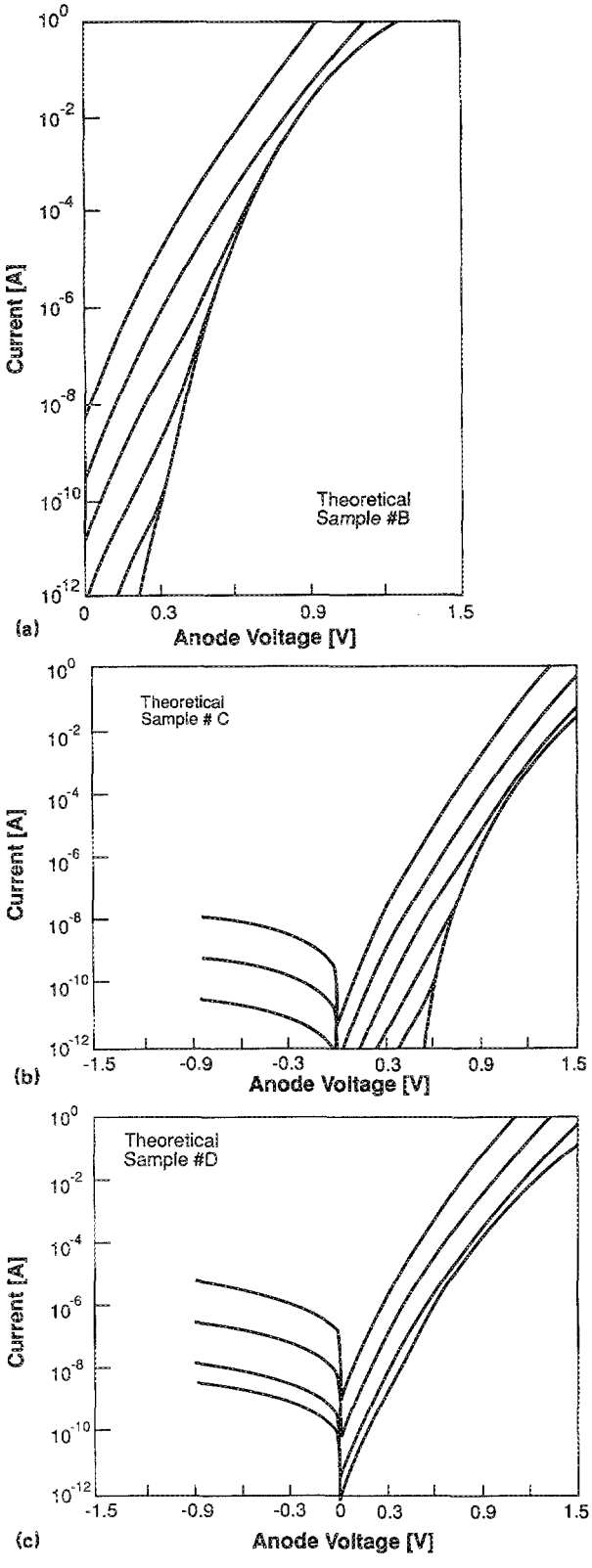

FIG. 7. Theoretical I-V characteristics at 77 K taking $E_1^{X_l} - E_0^{\Gamma}$ as a parameter. The values of $\Delta E_{c\Gamma\Gamma} = E_1^{\Gamma} - E_0^{\Gamma}$ and $\Delta E_{c\Gamma X} = E_1^{X_l} - E_0^{\Gamma}$ are assumed to be constant. Effective mass and prefactor values listed in Table II are used. (a) Sample B. The values of $E_1^{X_l} - E_0^{\Gamma}$ from the bottom are 0.35, 0.22, 0.20, 0.18, 0.16, 0.14 eV, respectively. $\Delta E_{c\Gamma\Gamma} = 0.28$ eV and $\Delta E_{c\Gamma X} = 0.35$ eV. (b) For sample C. Those are 0.32, 0.26, 0.24, 0.22, 0.20, 0.18, 0.16 eV, respectively. $\Delta E_{c\Gamma\Gamma} = 0.40$ eV and $\Delta E_{c\Gamma X} = 0.32$ eV. Two bottom curves at reverse bias are not shown here, because they are very small. (c) Sample D. Those are 0.20, 0.18, 0.16, 0.14 eV, respectively. $\Delta E_{c\Gamma\Gamma} = 0.75$ eV and $\Delta E_{c\Gamma X} = 0.20$ eV.

and experiment is, however, better for sample D, as shown in Figs. 4(d) and 7(c). This may be because, even though there exist impurities, the energy barrier to the conduction band is relatively smaller than those of samples B and C, so that current through X_l is dominant over the other mechanism, which can be evidenced by no such excess current at low temperature as observed for samples B and C.

V. CONCLUSIONS

Theoretical I-V characteristics of relatively thick semiconductor heterojunction barriers taking image force barrier lowering into account are calculated, and a procedure to extract parameters is proposed and applied. The parameters obtained from the zero stress I-V characteristics of n^+-GaAs–i-$Al_xGa_{1-x}As$–n-GaAs diodes grown on (100) n^+-GaAs substrates with $0.3 \leqslant x \leqslant 0.8$ and thicknesses from 300 to 400 Å agree well with those deduced from the previous results. The calculated temperature-dependent I-V characteristics using extracted parameters show good agreement with experimental results except at temperatures less than 100 K where excess current is observed. This anomaly is most probably due to tunneling through impurities in the AlGaAs layer.

Uniaxial stress dependence of I-V characteristics for ⟨100⟩ longitudinal stress is also measured at 77 K. These results show good agreement with calculations of thermionic emission (TE) and tunneling current (TU). The rate of change with stress of the band-edge energy difference between Γ in GaAs and X_l in AlGaAs is found to be 14 ± 2 meV/kbar, leading to an X-valley shear deformation potential of 9.6 ± 1.8 eV in AlGaAs, which is believed to be the most accurate measured value to date. However, for some samples, assumption of about 80 meV smaller absolute values of the band-edge difference between Γ in GaAs and X_l in AlGaAs are required to fit our theory to the experimental results. The explanation is discussed in Sec. IV.

ACKNOWLEDGMENTS

The support from the National Science Foundation through Contract No. NSF/ECS-8803928 and IBM are gratefully acknowledged. We also would like to thank Dr. F. O. Williamson for useful discussions.

[1] P. M. Solomon, C. M. Knoedler, and S. L. Wright, IEEE Electron Devices Lett. **EDL-5**, 379 (1984).
[2] P. M. Solomon, S. L. Wright, and C. Lanza, Superlattices Microstruct. **2**, 521 (1986).
[3] D. Delagebeaudeuf, P. Delescluse, P. Etienne, J. Massies, M. Laviron, J. Chaplart, and T. Linh, Electron. Lett. **18**, 85 (1982).
[4] A. R. Bonnefoi, Ph.D. Thesis, California Institute of Technology, Pasadena, California (1987).
[5] E. E. Mendez, E. Calleja, and W. I. Wang, Appl. Phys. Lett. **53**, 977 (1988).
[6] D. Landheer, H. C. Liu, M. Buchanan, and R. Stoner, Appl. Phys. Lett. **54**, 1784 (1989)
[7] H. C. Liu, Appl. Phys. Lett. **51**, 1019 (1987).
[8] P. J. Price, Surf. Sci. **196**, 394 (1988).
[9] H. Akera, S. Wakahara, and T. Ando, Surf. Sci. **196**, 694 (1988).
[10] A. C. Gossard, W. Brown, C. L. Allyn, and W. Wiegmann, J. Vac. Sci. Technol. **20**, 694 (1982).
[11] T. W. Hickmott, P. M. Solomon, R. Fischer, and H. Morkoc, Appl. Phys. Lett. **44**, 90 (1984).
[12] P. M. Solomon, T. W. Hickmott, H. Morkoc, and R. Fischer, Appl. Phys. Lett. **42**, 821 (1983).
[13] E. E. Mendez, E. Calleja, and W. I. Wang, Phys. Rev. B **34**, 6026 (1986).
[14] J. E. Smith, J. C. McGroddy, and M. I. Nathan, Phys. Rev. **186**, 727 (1969).
[15] P. M. Solomon, S. L. Wright, and D. La Tulipe, Appl. Phys. Lett. **49**, 1453 (1986).
[16] C. Pickering and A. R. Adams, J. Phys. C **10**, 3115 (1977).
[17] Previous to this work there were two reports of the measurement of Ξ that are cited in Ref. 18. Our measurement was first reported a few months ago and is cited in Ref. 27 of this paper.
[18] D. E. Aspnes and M. Cardona, Phys. Rev. B **17**, 741 (1978); S. Adachi, J. Appl. Phys. **58**, R1 (1985).
[19] See, for example, *Encyclopedia of Physics*, edited by S. Flugge (Springer, Berlin, 1956), Vol. 21.
[20] D. Delagebeaudeuf and N. T. Linh, IEEE Trans. Electron Devices **ED-29**, 955 (1982).
[21] K. Lee, M. S. Shur, T. J. Drummond, S. L. Su, W. G. Lyons, R. Fischer, and H. Morkoc, J. Vac. Sci. Technol. B **1**, 186 (1983).
[22] F. Stern and S. D. Sarma, Phys. Rev. B **30**, 840 (1984).
[23] J. Yoshida, IEEE Trans. Electron Devices **ED-33**, 154 (1986).
[24] Y. H. Byun, K. Lee, and M. Shur, Electron Device Lett. **EDL-11**, 50 (1990).
[25] M. Cuevas and H. Fritzsche, Phys. Rev. **137**, A1847 (1965).
[26] J. Batey and S. L. Wright, J. Appl. Phys. **59**, 200 (1986).
[27] S. S. Lu, K. Lee, M. I. Nathan, M. Heiblum, and S. L. Wright, Appl. Phys. Lett. **55**, 1336 (1989).
[28] U. Venkateswaran, M. Chandrasekhar, H. R. Chandrasekhar, B. A. Vojak, F. A. Chambers, and J. M. Meese, Phys. Rev. B **33**, 8416 (1986).
[29] D. J. Wolford and J. A. Bradley, Solid State Commun. **53**, 1069 (1985).
[30] T. F. Kuech, D. J. Wolford, R. Potemski, J. A. Bradley, and K. H. Kelleher, Appl. Phys. Lett. **51**, 505 (1987).
[31] T. N. Theis, in Proceedings of the International Conference on Shallow Impurities in Semiconductors, Linköping, Sweden, 1988.